

1 *Review*

2 **A Trajectory-Based Method to Explore Reaction** 3 **Mechanisms**

4 **Saulo A. Vázquez**¹, **Xose L. Otero**² and **Emilio Martínez-Núñez**^{1,*}

5 ¹ Departamento de Química Física, Facultade de Química, Campus Vida, Universidade de Santiago de
6 Compostela, 15782, Santiago de Compostela, Spain; saulo.vazquez@usc.es, emilio.nunez@usc.es

7 ² Unidade de Bioestadística, Facultade de Medicina, Universidade de Santiago de Compostela, 15782,
8 Santiago de Compostela, Spain; xoseluis.otero@usc.es

9 * Correspondence: emilio.nunez@usc.es; Tel.: +34-881814216

10

11 **Abstract:** The tsscds method, recently developed in our group, discovers chemical reaction
12 mechanisms with minimal human intervention. It employs accelerated molecular dynamics,
13 spectral graph theory, statistical rate theory and stochastic simulations to uncover chemical reaction
14 paths and to solve the kinetics at the experimental conditions. In the present review, its application
15 to solve mechanistic/kinetics problems in different research areas will be presented. Examples will
16 be given of reactions involved in photodissociation dynamics, mass spectrometry, combustion
17 chemistry and organometallic catalysis. Some planned improvements will also be described.

18 **Keywords:** automated algorithm; molecular dynamics; graph theory; statistical rate theory; kinetics
19 simulations.

20

21 **1. Introduction**

22 Theoretical studies of reaction mechanisms can greatly benefit nowadays by leveraging the
23 surge of automated methods developed in the last few years [1-58]. The idea of these new
24 computational protocols is to substitute human intervention by less error-prone and less tedious
25 automated algorithms. The automated methodologies range from chemical heuristics to the use of
26 artificial forces to boost chemical reactions.

27 Our group has contributed with the development of a method called tsscds [43-47], which is
28 based on accelerated molecular dynamics (MD), as are some others [29, 30]. In our trajectories, the
29 bonds of the molecule(s) are broken/formed thanks to large amounts of energy placed in each normal
30 mode/atom of the system [45]. The distinctive feature of tsscds compared to others is the primary
31 target of the post-processing analysis: the search for transition states (TS) rather than minima.
32 Additionally, having determined the TS of a given process, its rate can easily be determined using
33 transition state theory (TST) [59-62]. Thus, finding the relevant TSs on a given potential energy
34 surface (PES), as our method does, is a subject of fundamental importance in chemistry.

35 In tsscds, after completion of a trajectory, an algorithm named bond breaking/formation search
36 (BBFS) [45] is employed to select good TS guess structures, which are then optimized using
37 Eigenvector Following (EF) [63]. In particular, the adjacency matrix, which indicates whether pairs
38 of atoms form a bond, is monitored along each trajectory to identify the atoms/bonds involved in all
39 chemical reactions taking place. Then, for each of the selected candidates, a partial optimization is
40 firstly carried out by freezing the atoms involved in the reaction. The partially-optimized structure is
41 subsequently subjected to TS optimization using the EF algorithm. The resulting TSs are then
42 connected with the minima using intrinsic reaction coordinate (IRC) calculations [64]. Finally, tsscds
43 also features a Kinetic Monte Carlo [65] module that provides the desired kinetic information using
44 the network of TSs and minima. The source code can be downloaded from:
45 <http://forge.cesga.es/wiki/g/tsscds/HomePage>.

46 The method has been successfully employed to study reactions involved in combustion [66, 67],
47 photolysis [68-70], mass spectrometry [71] and organometallic catalysis [43]. The aim of this review
48 is to go over several examples where tsscds is employed to either discover new mechanisms and/or
49 to explain the experiments. For detailed comparisons among different methods for exploring reaction
50 space, the reader is referred to two recent reviews [58, 72]. Additionally, in the last section, some
51 planned improvements to enhance the efficiency/efficacy or to expand the scope of tsscds will be
52 described.

53 2. Method

54 The method tsscds has been recently put forward by one of the authors as an automated tool to
55 discover reaction mechanisms [44, 45]. The basic idea behind tsscds is to run accelerated MD
56 simulations with the aim to break/form bonds within a few hundred femtoseconds. The simulations
57 are called “accelerated” because the molecules experience breakage or formation of new bonds very
58 rapidly thanks to large amounts of vibrational energy placed in each normal mode of the system. In
59 particular, a range of vibrational energies of ~20-50 kcal/mol per normal mode is initially employed.
60 However, this range is automatically adjusted to attain at least 60% reactive trajectories in the MD
61 simulations. Although the default option is to excite all vibrational modes of the system (using
62 microcanonical normal mode sampling [73]), the user can decide to heat only one part of the system
63 selecting a few normal modes to be initially excited. The latter option can be particularly useful for
64 large systems.

65 The trajectory results are then analyzed with a post-processing algorithm (named BBFS), which
66 identifies geometries with partly formed/broken bonds. Those structures serve as TS candidates in
67 subsequent transition state optimizations. As detailed below, BBFS is based on the adjacency matrix,
68 a Graph Theory object that has been employed in other successful automated methods like the one
69 developed by Zimmerman [16]. Similar ideas have also been recently employed to analyze changes
70 in conformations occurring in MD simulations [74].

71 Once the TSs are optimized, a reaction network is constructed by computing the intrinsic
72 reaction coordinates (IRCs) [64] connecting TSs with intermediates [64]. The method employs two
73 levels of theory: semi-empirical and *ab initio*/DFT. The semi-empirical calculations are performed to
74 run the MD simulations and to obtain approximate TSs structures, while a higher level of theory is
75 used to re-optimize the TSs and run IRC calculations. Two different electronic structure programs
76 are employed: MOPAC2016 [75] and Gaussian09 [76] for the semi-empirical and *ab initio*/DFT
77 calculations, respectively.

78 Unlike other automated methods like GRRM [42], our methodology has been employed so far
79 to study only the ground electronic state. This is in part due to the fact that, currently, the potential
80 energy and gradients can only be calculated at the semiempirical level of theory. The following is a
81 description of the graph-theoretic tools and kinetic models employed in our method.

82 2.1. Graph Theory

83 A number of graph theoretic tools are employed at various stages of the procedure to find
84 transition states (TS), screen their structures and construct a reaction network. Specifically, the time
85 dependence of the adjacency matrix \mathbf{A} is employed to discriminate TS-like geometries along the
86 trajectories. The elements of this matrix are defined as:

$$87 \quad a_{ij} = \begin{cases} 1 & \text{if } r_{ij} < r_{ij}^{\text{ref}} \\ 0 & \text{otherwise} \end{cases} \quad (1)$$

88 with r_{ij} being the distance between atoms i and j , and r_{ij}^{ref} a reference value that sets the upper
89 limit for the bond length between the pair; in practice r_{ij}^{ref} is taken 20% greater than the sum of the
90 covalent radii of i and j [45]. Thus, for an N -atom system, \mathbf{A} is a $N \times N$ symmetric matrix with
91 zeros on its diagonal.

92 Additionally, a weighted adjacency matrix \mathbf{A}^w is also employed in tsscds, whose off-diagonal
93 elements are defined as:

$$94 \quad a_{ij}^w = \frac{1 - (r_{ij}/r_{ij}^{\text{ref}})^n}{1 - (r_{ij}/r_{ij}^{\text{ref}})^m} \quad (2)$$

95 Values of 6 and 12 have been employed in previous work for n and m , respectively [44]. Matrix \mathbf{A}^w
 96 contains information on the 3D geometry of the molecule,[77] and its eigenvalues and eigenvectors
 97 can be employed to construct the so-called SPRINT coordinates [77]. An important property of these
 98 coordinates is their invariance with respect to translation, rotation and permutation of atoms, which
 99 makes them good molecular descriptors in trajectory-based methods. SPRINT coordinates are
 100 employed in tsscds to remove redundant structures.

101 Another matrix employed to determine the number of fragments in the system is the Laplacian,
 102 which is defined as:

$$103 \quad \mathbf{L}^{(w)} = \mathbf{D} - \mathbf{A}^{(w)} \quad (3)$$

104 where \mathbf{D} is the so-called degree matrix [44], whose elements are defined as:

$$105 \quad d_{ij} = \begin{cases} \text{deg}(v_i) & \text{if } i = j \\ 0 & \text{otherwise} \end{cases} \quad (4)$$

106 where the degree $\text{deg}(v_i)$ of an atom counts the number of contacts. The superscript (w) on \mathbf{L} and
 107 \mathbf{A} indicates that the corresponding matrix can either be weighted or not. For a non-weighted graph,
 108 the lowest eigenvalue of the Laplacian λ_1 is always zero, and the total number of zero eigenvalues
 109 determines the number of fragments of the system. For a weighted graph, an upper threshold for λ_1^w
 110 is employed to identify fragmented structures [44]. The smallest non-zero eigenvalue is called the
 111 spectral gap, which is a measure of the degree of fragmentation of the structure. Thus, a small value
 112 of the spectral gap is associated with structures presenting non-covalent bonds (like van der Waals
 113 complexes), which are usually of no interest in chemical dynamics and kinetics.

114 The invariance of the SPRINT coordinates upon atom permutation is very important for the
 115 analyses of trajectories, where scrambling of atoms is frequent, as stated above. However, since the
 116 identity of each atom is absent in the adjacency matrix, SPRINT coordinates are identical for two
 117 structures where two non-equivalent atoms swap positions. For that reason, another type of
 118 molecular descriptor, based on a modified (weighted or not) adjacency matrix, is employed in tsscds.
 119 This new matrix, denoted as $\mathbf{A}_Z^{(w)}$, contains the atomic numbers Z_i of the atoms on the diagonal:

$$120 \quad a_{z,ij}^{(w)} = \begin{cases} a_{ij}^{(w)} & \text{if } i \neq j \\ 1 + \frac{Z_i}{10} & \text{if } i = j \end{cases} \quad (5)$$

121 The expression for the diagonal elements is chosen to provide values comparable to the off-
 122 diagonal ones. Most importantly, the eigenvalues of this new matrix are only invariant with respect
 123 to the permutation of like atoms, and it is widely employed in tsscds.

124 2.2. Kinetics simulations

125 The kinetics module of tsscds calculates rate constants for all the elementary steps and solves
 126 the set of first-order differential equations that describe the time evolution of all species (usually
 127 known as chemical master equation).

128 The rate constants can either be obtained as a function of temperature or energy. In the former
 129 case, transition state theory is employed [59-62]:

$$130 \quad k(T) = \sigma \frac{k_B T}{h} \left(\frac{RT}{p_0} \right)^{\Delta n} e^{-\frac{\Delta G^\ddagger}{RT}} \quad (6)$$

131 where σ is the reaction path degeneracy, T is the temperature, h is Planck's constant, ΔG^\ddagger is the
 132 free energy of activation, p_0 is 1 bar and $\Delta n = 1$ (0) for bimolecular (unimolecular) reactions. The
 133 reaction path degeneracy is calculated as $\sigma = \frac{m^{TS}}{m}$, where m and m^{TS} are the number of optical
 134 isomers of the reactant and transition states, respectively [78].

135 By contrast, the microcanonical rate constants are computed according to RRKM theory [78]:

$$k(E) = \sigma \frac{W^{TS}(E)}{h\rho(E)} \quad (7)$$

where $W^{TS}(E)$ is the sum of states at the TS, $\rho(E)$ is the density of states at the reactant, and E is the excitation energy of the system. The sums and densities of states are evaluated by direct count of the harmonic vibrational states using the Beyer-Swinehart algorithm. Once all state-to-state rates are determined, the chemical master equation is solved using Kinetic Monte Carlo simulations [65].

3. Overview of the applications of tsscds

The tsscds methodology has been employed in our lab to elucidate reaction mechanisms involved in photodissociation dynamics, mass spectrometry, combustion and organometallic catalysis, and in this section, several examples of each type are reviewed.

3.1. Photodissociation dynamics

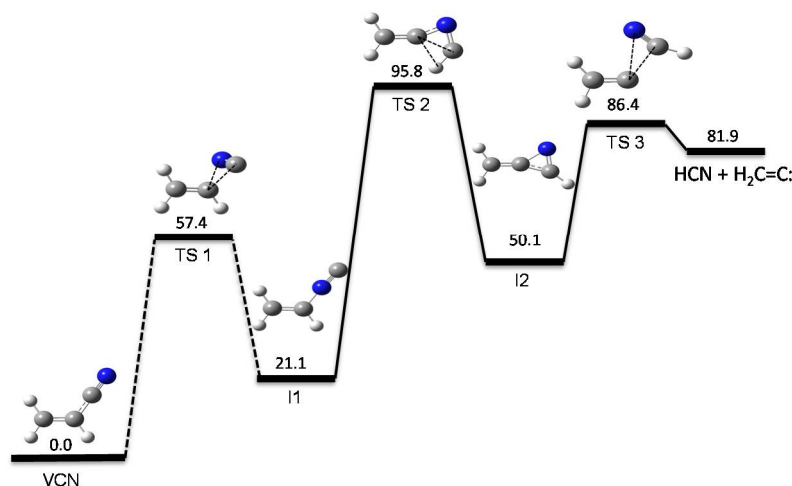
The dissociation of molecules can be promoted by using a laser source, which is known as photodissociation. Although many photodissociations take place in excited states, important mechanisms may occur in the ground electronic state following internal conversion. One of the quantities of interest is the product yield, which is usually determined in the experiments. The understanding of the dissociation channels in organic compounds has greatly benefited from the interplay between photolysis experiments and computational studies [70, 79-92].

In this section, we summarize the results obtained with our automated method for systems that have also been studied in photodissociation experiments, highlighting the most important conclusions. In particular, the dissociation channels of formaldehyde, formic acid, vinyl cyanide, acrolein, acryloyl chloride and methyl cyanofornate were studied with our tsscds methodology.

Formaldehyde was employed as a benchmark system to test tsscds. The system had been previously studied with other automated methods like the scaled hypersphere search [33] and the global reaction route mapping (GRRM) [35]. The results obtained with all algorithms are comparable, and the kinetically-relevant stationary points are found using any procedure.

The study of the dissociation channels of formic acid (CO_2H_2) with tsscds revealed the existence of a new TS for the water-gas shift reaction (WGSR: $\text{CO} + \text{H}_2\text{O} \rightarrow \text{CO}_2 + \text{H}_2$) [45]. By contrast, GRRM predicted three consecutive steps for the shortest path of the WGSR [35]. The discovery of the new TS is a consequence of the highly non-IRC [93] nature of the trajectories employed in tsscds [45]; in other words, IRC jumps are not uncommon events [94]. This exemplifies one of the advantages of using trajectory-based methods to discover new reactions: we are not restricted to unimolecular reactions and the only constrain to discover new processes is the molecular formula of the system. Additionally, the large amounts of vibrational energy put in the normal modes enhances configurational space sampling in tsscds, which permits the exploration of all types of reactions.

Our automated computational study on the dissociation of vinyl cyanide (VCN) [70] provides a HCN/HNC branching ratio in nearly perfect agreement with experiments for an excitation energy of 148 kcal/mol [95]. Besides the traditional 3-center and 4-center elimination mechanisms found in many HX eliminations from $\text{CH}_2=\text{CHX}$ systems, a new HCN elimination pathway involving three TSs was discovered in the tsscds study. The new mechanism involves three TSs and two intermediates and is shown in Figure 1.



176

177

178

179

180

Figure 1. New HCN elimination mechanism from VCN obtained with tsscads. The numbers are relative energies (including the zero-point vibrational energy) with respect to VCN, calculated at the CCSD(T)/6-311++G(3df,3pd)//CCSD/6-311+G(2d,2p) level of theory with the vibrational frequencies obtained using CCSD/6-311+G(2d,2p) numerical Hessians.

181

182

183

184

185

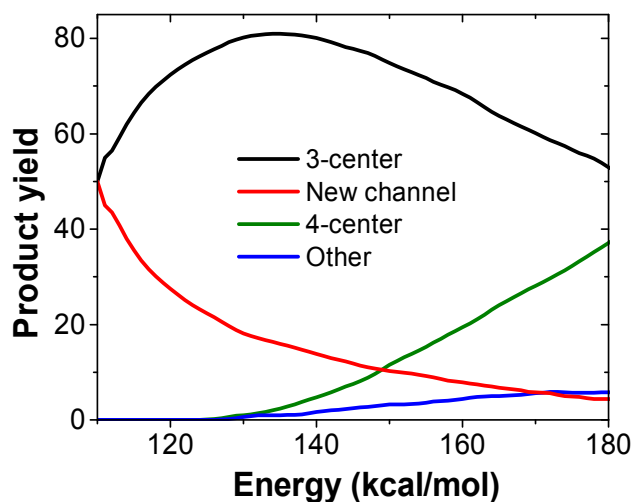
Although alternative routes for HX elimination were also found for other ethylene analogues, those pathways involved high-energy TSs and were not competitive with the conventional 3-center and 4-center channels. This was the first time a new HX elimination channel competes with the well-known 3-center and 4-center processes in the dissociation of $\text{CH}_2=\text{CHX}$ species.

186

187

188

Figure 2 shows the product yields as a function of excitation energy obtained in our kinetic simulations from VCN. As seen in the figure, at low excitation energies (<150 kcal/mol) the new channel (red) is more important than the 4-center channel (green) and accounts for half of the HCN eliminations when the excitation energy is 110 kcal/mol.



189

190

Figure 2. Kinetic simulation results of the different HCN elimination channels from VCN.

191

192

193

194

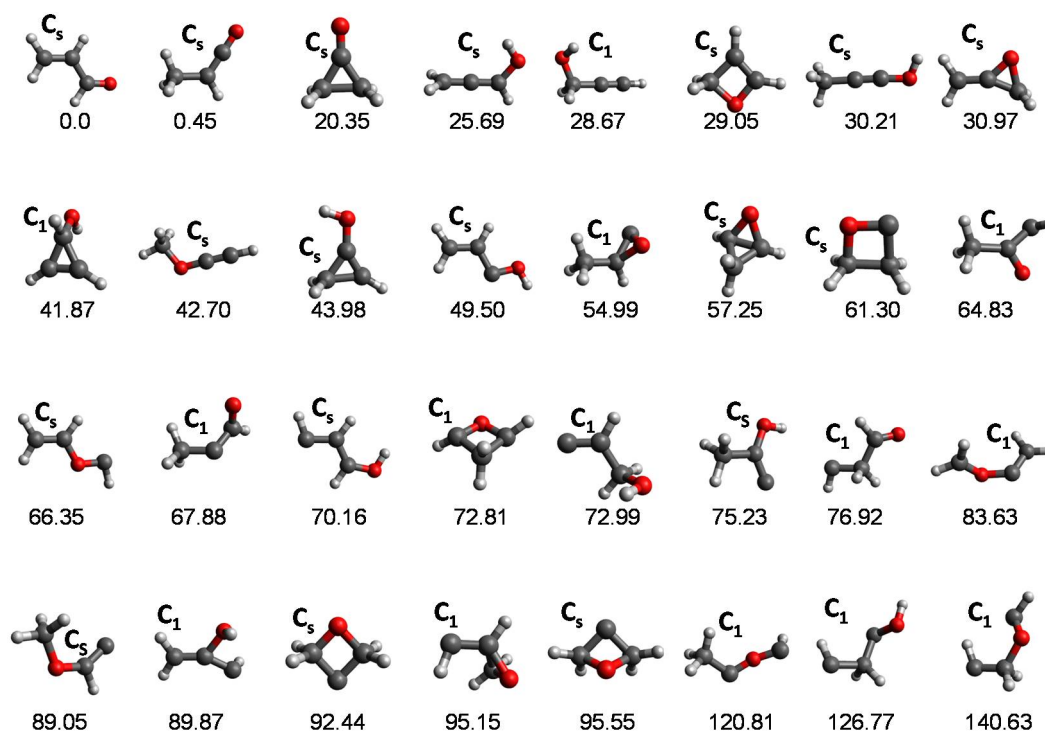
195

196

197

The tsscads methodology was also employed to study the dissociation of acrolein (ACRL, $\text{C}_3\text{H}_4\text{O}$), which comprises many different fragmentation channels involving more than 250 transition states and 66 minima [44]. This system was studied with an enhanced procedure (now fully integrated in the method) consisting in the initialization of the MD simulations from multiple minima. In this new procedure the method works in an iterative manner. In the first iteration all MD simulations start from a starting structure, but once some TSs and intermediates are located, subsequent iterations utilize not only the starting equilibrium structure but also the newly generated intermediates to

198 initialize the MD simulations. Compare to a single-minimum initialization, the use of multiple
 199 minima to start the dynamics ensures a better sampling of the PES of the system.



200

201 **Figure 3.** Minima obtained by tsscads for the C₃H₄O system. The structures are arranged in ascending
 202 order of their relative energies (shown at the bottom of each structure), which are obtained at the
 203 CCSD(T)/6-311+G(3df,2p)//B3LYP/6-311G(d,p) level of theory. Conformers are not included in the
 204 figure and only the lowest lying of each family is displayed.

205 The potential energy surface of the C₃H₄O system is very complex and the 32 equilibrium
 206 structures (not including conformers) shown in Figure 3 were found with tsscads, with ACRL being
 207 the global minimum. To exemplify the importance of automated reaction discovery methods, we
 208 compare our results with those obtained by Chin et al. [96], who manually located equilibrium
 209 structures and TSs. Using the same levels of theory as in our study, Chin et al. only found 6 of the 66
 210 minima obtained with tsscads. Most importantly, the relative product abundances obtained with
 211 tsscads at 148 kcal/mol (the energy corresponding to the experimental wavelength of 193 nm) are much
 212 closer to the experimental results than the computational results of Chin et al., as seen in Table 1.

213

214

Table 1. Relative product abundances obtained by different computational studies and experiment in the photodissociation of ACRL at 193 nm.

Channel	Chin et al. [96]	tsscads	Exp [97]
H ₂ O	0.01	0.03	0.07
CH ₂ O	0.65	0.20	0.07
H ₂	0.09	0.19	0.00
CO	1.00	1.00	1.00
H ₂ +CO+HCCH	6.82	1.49	1.10

215

216

217

218

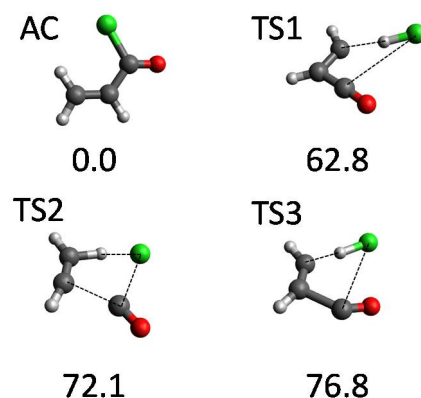
219

220

221

Another system that attracted our attention was acryloyl chloride (AC). Overall, around 700 stationary points were found using our tsscads strategy. Of all possible dissociation channels from AC, experiments focus on the HCl dissociations. The use of our automated procedure led to the discovery of the three new HCl dissociation TSs [69] displayed in Figure 4; the figure also shows the AC equilibrium structure. The highest-energy TSs (TS2 and TS3) correspond to three-body dissociations leading to acetylene, carbon monoxide and hydrogen chloride, and they only become important at

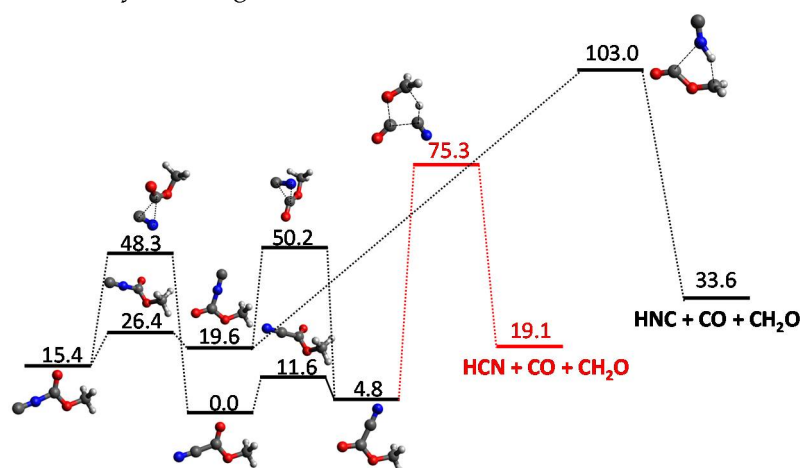
222 high excitation energies. By contrast, HCl elimination over TS1 is predominant at the experimental
 223 conditions (148 kcal/mol) [98], showing again that tsscdis capable of finding competitive pathways.



224

225 **Figure 4.** Structure of AC minimum and the three new TSs found with tsscdis for the HCl elimination
 226 from AC. Numbers are relative energies in kcal/mol (including the zero-point vibrational energy)
 227 with respect to AC, calculated at the CCSD(T)/6-311+G(3df,2p)//B3LYP/6-311+G(2d,2p) level of
 228 theory.

229 Finally, with the aim of exploring possible sources of HCN and HNC in astrophysical
 230 environments, the dissociation channels of methyl cyanoformate (MCF) were probed with tsscdis,
 231 excited state calculations and photolysis experiments [68]. In particular, time-resolved infrared
 232 spectroscopy measurements indicate that both HCN and HNC are formed after the 193-nm
 233 photolysis of MCF [68]. The excited state calculations suggest that most of the dissociations take place
 234 in the S_2 excited state leading to $\text{CH}_3\text{O} + \text{NCCO}$ via a Norrish type I reaction, in agreement with
 235 experiment. However, our calculations are also consistent with cascading internal conversion from
 236 S_2 to produce vibrationally excited ground state MCF.



237

238 **Figure 5.** Relevant HCN and HNC pathways in the ground-state PES of methyl cyanoformate for an
 239 excitation energy of 148 kcal/mol. Relative energies (in kcal mol⁻¹) include ZPE contributions and
 240 were obtained by CCSD(T)/6-311+G(3df,3pd)//MP2/6-311+G(2d,2p) calculations.

241 To study the dissociation of vibrationally excited MCF molecules in the S_0 electronic state, tsscdis
 242 was employed. Our approach assumes that, after the internal conversion process, intramolecular
 243 vibrational redistribution is fast enough to ensure RRKM behavior. With the tsscdis procedure several
 244 HNC and HCN mechanisms are found, and Figure 5 shows the kinetically-relevant ones at 148
 245 kcal/mol. The kinetic simulations predict a HNC/HCN branching ratio of 0.01, which is in
 246 semiquantitative agreement with that determined in the experiments (≈ 0.07). The work provides

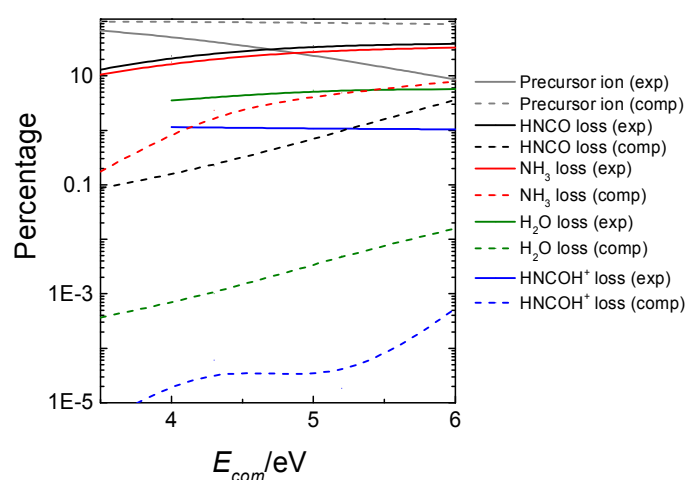
247 further insights into the intriguing observation of overabundance of HNC in astrophysical
248 environments.

249 3.2. Mass spectrometry

250 The prediction of mass spectra remains much of a challenge for the community of computational
251 chemists. The common computational approaches employed for such endeavor include statistical
252 rate theory calculations, MD simulations and electronic structure calculations [99-113]. Our
253 automated method is very useful in this regard and can easily be coupled with MD simulations of
254 collisions to generate theoretically-based mass spectra as described below.

255 In particular, tsscds was employed to simulate mass spectrometry (MS) experiments of
256 protonated uracil, [uracil]H⁺. Our computational results indicate that the decomposition of [uracil]H⁺
257 involves more than one thousand stationary points and 751 elementary reactions [71]. Branching
258 ratios for the different fragmentation channels can be automatically obtained from tsscds. However,
259 these fractions are a function of the ion's internal energy and cannot be directly compared with MS
260 experiments, where the collision energy in the center-of-mass framework (E_{com}) is employed instead.
261 For that reason the tsscds results were combined with collisional dynamics simulations [71], which
262 provide the fraction of E_{com} transferred to the ion's internal energy.

263 The resulting computationally-predicted product abundances (dashed lines) are compared in
264 Figure 6 with the experimental ones (solid lines). As seen in the figure, for the predominant
265 dissociation channels, the computationally-predicted product abundances are in qualitative
266 agreement with experiment, and formation of HNCO (black), NH₃ (red), H₂O (green) and HNCOH⁺
267 (blue) are the major channels. Discrepancies with experiment can be attributed to the possible
268 existence of well-known non-statistical behavior in many collision-induced dissociations [100, 114],
269 which cannot be captured with our statistical model.



270
271 **Figure 6.** Experimental (exp) and calculated (comp) intensities of precursor and fragment ions
272 produced in the fragmentation of protonated uracil.

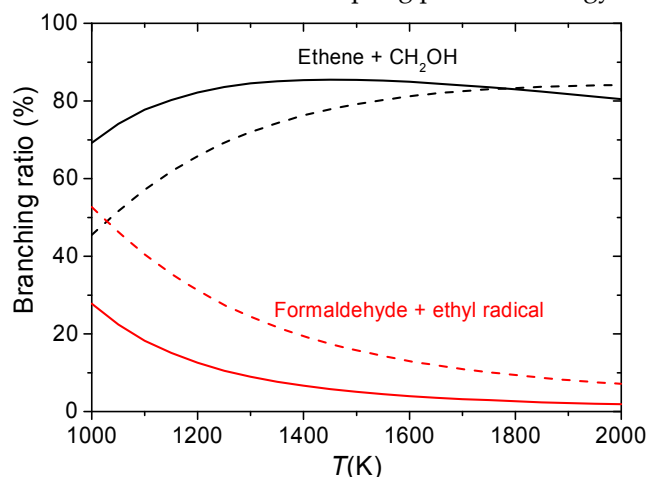
273 3.3. Combustion chemistry

274 Modeling the combustion reactions of oxygenated fuels is of great interest due to their potential
275 use as alternatives to conventional petroleum-based fuels. To investigate combustion mechanisms, it
276 is important to use kinetic models and perform computer simulations as a complement to
277 experimental determinations, due to the tremendous complexity of these chemical processes. In
278 general, different approximations are employed in combustion simulations to handle the complicated
279 mechanisms. One of these simplifications consist of considering only the lowest energy rotamers of
280 the involved species, which can lead to large errors in the calculation of rate coefficients.

281 In a recent paper, our group analyzed the influence of multiple conformers and paths in the
282 evaluation of rate constants and relative abundances of products formed in the thermal

283 decomposition of 1-propanol radicals using different methodologies including tsscds [66].
284 Specifically, the most relevant pathways reported in the literature [115-121] are obtained with tsscds,
285 except for the barrierless dissociation leading to propene + OH, since the present version of tsscds
286 cannot handle this type of reactions. Of significance, an important number of reactant and TS
287 conformers, not described in the previous studies, are obtained with tsscds.

288 A conformational reaction channel (CRC) was defined in our study [66] as the group of all the
289 paths that connect the conformers of a given reactant with the corresponding TS conformers. The
290 influence of these conformers on the rate constants and branchings ratios was investigated in detail
291 [66]. To study such influence, the output of tsscds (families of CRCs) was fed into a computer program
292 to treat torsional anharmonicity named Q2DTOR (also developed in our group) [122]. The results
293 obtained with tsscds and Q2DTOR were finally employed to calculate variational transition state
294 theory (VTST) [123-125] rate constants for all the CRCs. The multipath (MP) approach within VTST
295 was employed [125-129], where the rate constant of a given CRC is calculated using contributions
296 from all the conformers and paths. For comparison purposes the simplest one-well (1W) approach is
297 also considered; in the 1W method only the most stable conformers of reactant and TS are considered.
298 As seen in Figure 7, the product abundances obtained in the temperature range 1000-2000 K are
299 greatly influenced by the selected approach (MP vs 1W), particularly for the major products: ethene
300 + CH₂OH and formaldehyde + ethyl radical [66]. Our results show the importance of using automated
301 codes for discovering reaction mechanisms and sampling potential energy surfaces.



302

303 **Figure 7.** Branching ratios obtained in the kinetics simulations starting from one of the isomers of 1-
304 propanol (only the two major mechanisms are shown). The solid and dashed lines correspond to the
305 MP and 1W results, respectively.

306 Very recently, Fenard et al. developed a detailed kinetic model of the low-temperature oxidation
307 of tetrahydrofuran (THF) based on theoretically-calculated rate constants [67]. The reaction pathways
308 involved in these processes were probed with our automated software tsscds [67] using CBS-QB3 as
309 the choice for the high-level of electronic structure. The rate constants were determined using TST
310 with a tunneling correction using an Eckart potential.

311 The predictions from the model developed by Fenard et al. are overall in good agreement with
312 the different experimental measurements. Namely, it reproduces ignition delay times obtained in a
313 rapid-compression machine and in a shock tube, as well as numerous product mole fractions
314 measured in a jet-stirred reactor.

315 3.4. Organometallic catalysis

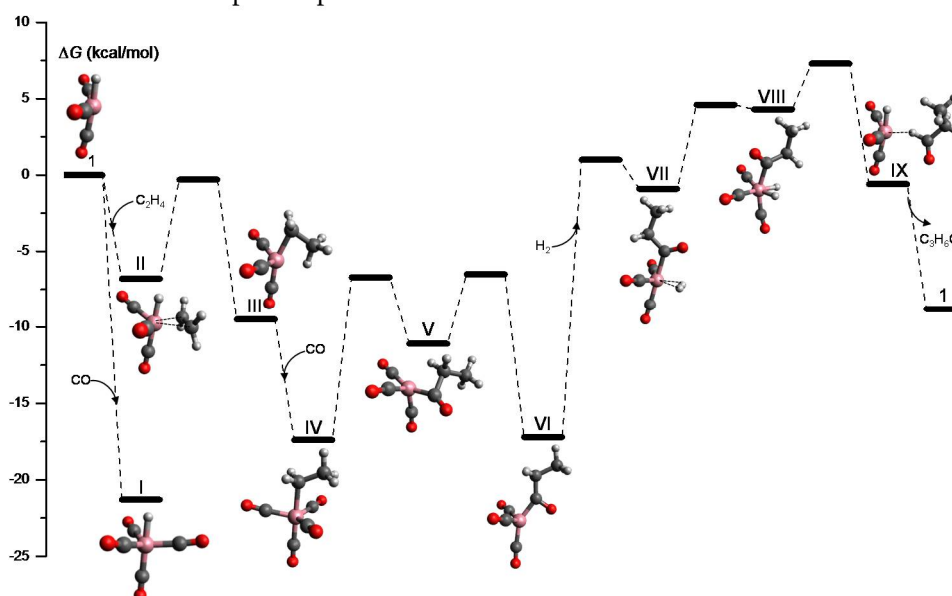
316 Computational studies of organometallic catalysis are becoming increasingly more important
317 because they can help elucidate reaction mechanisms, characterize catalytic intermediates,
318 supplement experimental studies, and also because of their predictive power [124, 130-133].

319 However, the traditional workflow of most computational studies consists of using chemical
320 intuition in the design of reaction routes and construction of guess TS structures. In recent years the
321 appearance of powerful automated computational methods to study homogenous catalysis [27, 43,
322 134-136] very much eased the tedious work of manual searches.

323 To exemplify the use of tsscds in organometallic catalysis, the cobalt-catalyzed
324 hydroformylation of ethylene was chosen [43]. Very briefly, the first step in our computational study
325 was to generate all combinations of the catalyst $\text{Co}(\text{CO})_3$ with any of the starting materials (CO , H_2
326 and ethylene), which in this case amounts to eight. Each of these combinations has fewer atoms than
327 the overall system and they were named sub-systems in our original paper [43]. Standard tsscds is
328 then run in each sub-system to build the reaction networks. Finally, the full reaction network is
329 obtained after merging the individual results for each sub-system.

330 Figure 8 shows the tsscds-calculated free energy profile for the formation of propanal ($\text{C}_3\text{H}_6\text{O}$),
331 which is the predominant channel; the level of theory employed was B3LYP/6-31G(d,p). As pointed
332 out in the original paper, this is not the best electronic structure method for this system and it was
333 only selected for comparison purposes. Additionally, we simulated the reactivity in the gas phase
334 because, for this system, solvent effects are unimportant [43, 133].

335 The mechanism shown in Figure 8 was obtained in an automated manner, and agrees with the
336 one predict by Heck and Breslow in the 1960s [137] and with more recent mechanistic studies [133].
337 This is a very interesting result as we needed to make no assumptions in our automated calculations.
338 Additionally, our method predicts that hydrogenation of ethylene is a side reaction that can be
339 predominant under low CO partial pressures.



340

341 **Figure 8.** Free energy profile for the Co-catalyzed hydroformylation of ethylene obtained in our tsscds
342 study using DFT calculations [133].

343 With the full reaction network constructed, the kinetics simulation module of tsscds can provide
344 a rate law for the hydroformylation reaction when a range of different initial conditions for each
345 species is employed. The kinetics calculations consist of transition state theory calculations [59-62] for
346 the thermal rate constants at 423 K, and subsequent Monte Carlo simulations using different initial
347 conditions of the reactants. Table 2 shows the orders of the catalyst and starting materials for the
348 hydroformylation reaction obtained experimentally [138], with tsscds [43], using a kinetic model
349 based on highly-accurate electronic structure calculations by Harvey and co-workers [133], and
350 obtained from another automated method by Habershon [27].

351 As seen in Table 2, tsscds agrees rather well with experiment and with the results obtained by
352 Harvey and co-workers [133]. Moreover, tsscds agrees much better with experiment than the other

353 automated method does [27] (last column of Table 2), despite the fact that both employ the same
 354 alkene, initial conditions for the kinetics, and level of theory for the electronic structure calculations.

355 **Table 2.** Orders of the hydroformylation reaction with respect to the catalyst and starting materials.

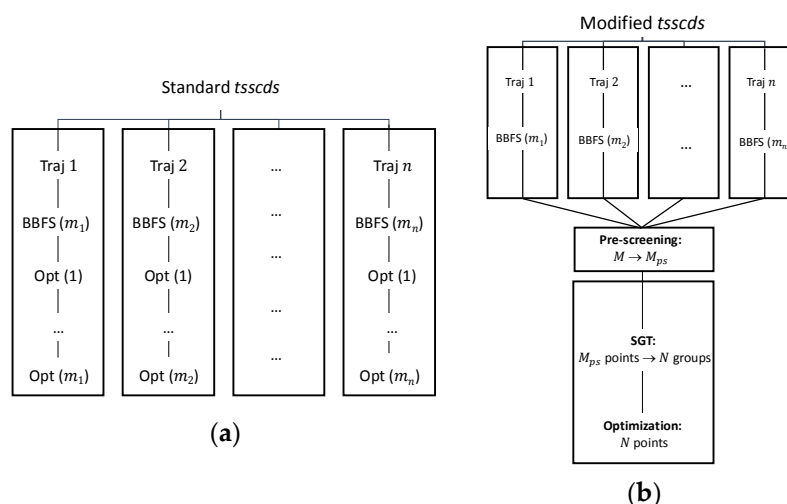
Species	Exp [138]	tsscads [43]	Harvey [133]	Habershon [27]
H ₂	0.6	0.4	0.5	1
CO	<0	<0	<0	<0
catalyst	0.8	0.5	0.5	1
alkene	1	1	1	0.55

356 4. Improvements

357 In this section we describe some improvements we plan to implement in the near future. They
 358 include: the use of Spectral Graph Theory, implementation of knowledge-based methods,
 359 implementation of rare event acceleration MD simulations, interface with other electronic structure
 360 codes, reparametrization of semiempirical methods, and the study of condensed phase reactions.

361 4.1. Use of Spectral Graph Theory to minimize the number of Hessian calculations

362 In standard tsscads, every single structure obtained after the BBFS analysis is subjected to TS
 363 optimization [45]. As seen in Figure 9(a), for a trajectory i , BBFS selects m_i TS candidates, which
 364 results in $M = \sum_{i=1}^n m_i$ optimizations, where n is the total number of trajectories. On the one hand,
 365 these M optimizations are the most CPU-time consuming step of the procedure as they involve
 366 Hessian calculations, while the integration of the trajectories only requires gradients. On the other
 367 hand, a number of those optimizations are repeated. This is so because trajectories visit more often
 368 those areas of the configurational space around the kinetically most relevant TSs, leading to multiple
 369 optimizations of those structures.
 370



371 **Figure 9.** (a) Original tsscads showcasing an example with n different trajectories resulting in a total
 372 number of $M = \sum_{i=1}^n m_i$ optimizations. (b) Modified tsscads showcasing the same example as in panel
 373 (a) with n different trajectories resulting in a total number of N optimizations.

374 The workflow of the enhanced procedure is shown in Figure 9(b). Briefly, instead of carrying
 375 out the optimizations for every single structure selected by the BBFS algorithm (as in the original
 376 implementation), the new procedure will run the MD simulations and store at once the M structures
 377 for the analysis of all trajectory data. This analysis will consist of a pre-screening, a Spectral Graph
 378 Theory (SGT) step, and the final optimization step.

379 Upon completion of the MD simulations, a pre-screening of the M structures will be performed
 380 based on the eigenvalues of the Laplacian matrix [44]. As pointed out above, the lowest eigenvalues

381 of this matrix indicate the degree of fragmentation of the molecular system. We aim here to discard
382 highly fragmented structures, i.e., TSs connecting van der Waals complexes, usually of negligible
383 relevance in a kinetics study. In the SGT step the remaining points will be partitioned into N groups
384 according to the eigenvalues of a TS adjacency matrix, calculated as the average of the reactant and
385 product adjacency matrices. Finally, we will select the closest point (geometry) to the centroid of each
386 cluster for optimization. With this new scheme the gain in efficiency can easily be quantified as the
387 reduction in the number of optimizations from M to N .

388 4.2. Implementation of knowledge-based mechanism generators

389 A number of reaction discovery methods are based on the so-called chemical heuristics [23, 48-
390 50]. In these methods, molecules are typically represented as graphs, in pretty much the same way as
391 in tsscds. Then, by applying transformations, based on encoded rules or principles inspired by
392 organic chemistry, to the reactant molecule graph, reactions, products and intermediates can readily
393 be obtained. Compared to MD-based methods, heuristic-based methods are less CPU-time
394 demanding.

395 Our idea will be to combine a heuristic-based bias in the MD simulations alongside with our
396 BBFS algorithm to obtain TSs. In particular, having defined a set of encoded rules based on chemical
397 knowledge, every single MD simulation will suffer a different bias, aimed to trigger a particular
398 reaction mechanism. In this way, the problem of multiple optimizations of a given TS mentioned
399 above would be minimized, if not completely avoided. The bias (analytical) potentials will be added
400 on top of the semiempirical potential to steer the dynamics towards a particular intermediate or
401 product.

402 4.3. Implementation of rare-event acceleration MD methods

403 One of the shortcomings of tsscds is the fact that chemical reactions are triggered by using very
404 high energies in the MD simulations. While this approach was successfully employed to tackle
405 different problems, it is biased towards the entropically favored reaction pathways. To alleviate this
406 drawback of the method we propose to replace the current MD strategy by the rare-event acceleration
407 method named Boxed Molecular Dynamics (BXD) [139]. BXD has its roots in work done by one of us
408 and D. Shalashilin more than a decade ago [140]. It introduces several reflective barriers in the phase
409 space of a MD trajectory along a particular collective variable. Those boundaries are employed to
410 push the dynamics along the collective variable into regions of phase space which would be rarely
411 sampled in an unbiased trajectory. However, the use of BXD constrains in configuration space suffers
412 from the same “entropic” bias mentioned above.

413 A generalization of BXD has been very recently put forward by Glowacki and co-workers [141].
414 They show that the BXD bias can also be introduced along the potential energy (E) of the system,
415 which is referred to as BXDE. By scanning through potential energy “boxes”, the energetic
416 “windows” at which different chemical reaction channels switch on or off can be identified. The
417 software design of tsscds is highly modular, which means that interfacing it with BXDE only requires
418 little effort, like the need of compatible input/output geometry formats in both codes and the use of
419 extra keywords in tsscds.

420 4.4. Interface with other electronic structure codes

421 At present tsscds has been only interfaced with the MOPAC2016 [75] and the G09 [76]
422 electronic structure packages. The MD simulation employs gradients calculated at the semiempirical
423 level of theory, and the optimization step is carried out at both the semiempirical level with
424 MOPAC2016 and using higher levels (ab initio/DFT) with G09. Although we plan to reparametrize a
425 semiempirical Hamiltonian for use in organometallic catalysis (see below), we do not want to be
426 limited to this low-level electronic structure calculations. Therefore, we will use the ASE package [142]
427 to interface tsscds with other electronic structure codes like NWCHEM [143] or ORCA [144].
428

4.5. Reparametrization of semiempirical methods

The application of the tsscds method relies on the use of semiempirical Hamiltonians for exploring potential energy surfaces. For this reason, it is important that the semiempirical method provides a reasonably accurate representation of the system under investigation. Although significant improvements in these methods have been made over the last years [145], there are still known limitations, which claim for further developments and more accurate parametrizations. Two important limitations concern the non-covalent interactions for large systems and ligand dissociation energies for transition metal complexes. In both cases, the performance of the semiempirical methods is, in general, quite poor. Our goal is therefore to improve the description of both non-covalent interactions and transition metal complexes in PM7.

Regarding non-covalent interactions, we aim to develop an analytical correction for PM7. To this end, we will consider a set of small molecules, which are representative of the most important functional groups. All pairs of molecules will be considered to calculate interaction energies at three levels of theory: coupled-cluster (CC), DFT and PM7. For every pair, various orientations will be considered, each one emphasizing a different two-body interaction.

Then, sums of two-body Buckingham potentials (supplemented with damping functions for the dispersion) will be fit to the CC, DFT and PM7 interaction energies using our genetic algorithm program GAFit [146]. Finally, the resulting potentials $V_{\text{fit,CC}}$, $V_{\text{fit,DFT}}$ and $V_{\text{fit,PM7}}$ will be employed to build corrections V_X^{corr} to the PM7 interaction energies:

$$V_X^{\text{corr}} = V_{\text{fit,X}} - V_{\text{fit,PM7}} \quad (8)$$

where X is either CC or DFT. Whereas the $V_{\text{DFT}}^{\text{corr}}$ correction term will be employed to validate this methodology as explained below, the highly-accurate $V_{\text{CC}}^{\text{corr}}$ correction will be used once the validation succeeds.

The correction will be added to the PM7 energy V_{PM7} so that the PM7 Hamiltonian corrected for non-covalent (nc) interactions would read:

$$V_{\text{PM7,X}}^{\text{nc}} = V_{\text{PM7}} + V_X^{\text{corr}} \quad (9)$$

The strategy of using small representative molecules and sums of two-body functions was successfully employed in the development of intermolecular potentials for interactions of protonated peptides and silyl ions with perfluoroalkane self-assembled monolayers [147, 148]. Nevertheless, this strategy will be validated for the new functional groups by running DFT calculations for large systems. This will allow us to compare the DFT-calculated energies with those obtained with $V_{\text{PM7,DFT}}^{\text{nc}}$.

The semiempirical methods, and particularly PM6 and PM7, do not perform well for transition-metal complexes [149]. Our strategy here will be to reoptimize the PM7 Hamiltonian as in previous studies of our group (e.g., see ref. [68]). We will select popular transition metals and ligand molecules used in organometallic catalysis, and will carry out high-level ab initio calculations for our own benchmark database. To gain flexibility in the parametrizations, we will consider the possibility of defining "atom types" for the ligand atoms, depending on the functional groups, in much the same way as that done for the parametrization of the hpCADD NDDO Hamiltonian [150].

4.6. Study of condensed phase reactions

Our method is not limited to gas phase reactions. Although currently it only handles reactions in the gas phase, its modular design allows for a smooth adaptation of tsscds to deal with condensed phase reactions. For instance, to study solvent effects, the easiest way would be to use an implicit model, which in practice would only entail adding the appropriate keywords to the templates employed for the different electronic structure programs.

On the contrary, if one wants to use explicit solvent molecules, the MD module must be changed or substituted. At present, the MD module is a modified version of DRC routine in MOPAC2016, which includes different strategies for enhanced sampling, as detailed in the tutorial of tsscds [47]. To include solvent molecules in the MD simulations, one possibility would be to use CHARMM [151]

478 or to adapt DR. Finally, if the interest is a gas surface reactions, VENUS [152] would be the choice
479 to run the MD simulations because the authors have vast experience using this program.

480 **Author Contributions:** Writing-Review & Editing, S. A. V., X. L. O. and E.M.-N.

481 **Funding:** This research was funded by “Consellería de Cultura, Educación e Ordenación Universitaria, Xunta
482 de Galicia”, grant number ED431C 2017/17”, and by “Ministerio de Economía y Competitividad of Spain”, grant
483 number CTQ2014-58617-R.

484 **Acknowledgments:** The authors thank “Centro de Supercomputación de Galicia (CESGA)” for the use of their
485 computational facilities.

486 **Conflicts of Interest:** The authors declare no conflict of interest. The funders had no role in the design of the
487 study; in the collection, analyses, or interpretation of data; in the writing of the manuscript, and in the decision
488 to publish the results.

489

490 References

- 491 1. Schlegel, H. B., Geometry optimization. Wiley Interdisciplinary Reviews: Computational Molecular
492 Science **2011**, 1, 790-809.
- 493 2. Davis, H. L.; Wales, D. J.; Berry, R. S., Exploring potential energy surfaces with transition state
494 calculations. *J. Chem. Phys.* **1990**, 92, 4308-4319.
- 495 3. Sun, J. Q.; Ruedenberg, K., Gradient Extremals and Steepest Descent Lines on Potential Energy
496 Surfaces. *J. Chem. Phys.* **1993**, 98, 9707-9714.
- 497 4. Tsai, C. J.; Jordan, K. D., Use of an eigenmode method to locate the stationary points on the potential
498 energy surfaces of selected argon and water clusters. *J. Phys. Chem.* **1993**, 97, 11227-11237.
- 499 5. Abashkin, Y.; Russo, N., Transition state structures and reaction profiles from constrained
500 optimization procedure. Implementation in the framework of density functional theory. *J. Chem. Phys.*
501 **1994**, 100, 4477-4483.
- 502 6. Bondensgard, K.; Jensen, F., Gradient Extremal Bifurcation and Turning Points: an Application to the
503 H₂CO Potential Energy Surface. *J. Chem. Phys.* **1996**, 104, 8025-8031.
- 504 7. Doye, J. P. K.; Wales, D. J., Surveying a potential energy surface by eigenvector-following. *Zeitschrift
505 für Physik D Atoms, Molecules and Clusters* **1997**, 40, 194-197.
- 506 8. Quapp, W.; Hirsch, M.; Imig, O.; Heidrich, D., Searching for Saddle Points of Potential Energy Surfaces
507 by Following a Reduced Gradient. *J. Comput. Chem.* **1998**, 19, 1087-1100.
- 508 9. Černohorský, M.; Kettou, S.; Koča, J., VADER: New Software for Exploring Interconversions on
509 Potential Energy Surfaces. *J. Chem. Inf. Comput. Sci.* **1999**, 39, 705-712.
- 510 10. Westerberg, K. M.; Floudas, C. A., Locating all transition states and studying the reaction pathways of
511 potential energy surfaces. *J. Chem. Phys.* **1999**, 110, 9259-9295.
- 512 11. Wales, D. J.; Doye, J. P.; Miller, M. A.; Mortenson, P. N.; Walsh, T. R., Energy Landscapes: From
513 Clusters to Biomolecules. *Adv. Chem. Phys.* **2000**, 115, 1-111.
- 514 12. Iríkura, K. K.; Johnson, R. D., Predicting unexpected chemical reactions by isopotential searching. *J.
515 Phys. Chem. A* **2000**, 104, 2191-2194.
- 516 13. Müller, E. M.; Meijere, A. d.; Grubmüller, H., Predicting unimolecular chemical reactions: Chemical
517 flooding. *J. Chem. Phys.* **2002**, 116, 897-905.
- 518 14. Dallos, M.; Lischka, H.; Ventura Do Monte, E.; Hirsch, M.; Quapp, W., Determination of Energy
519 Minima and Saddle Points Using Multireference Configuration Interaction Methods in Combination
520 with Reduced Gradient Following: The S₀ surface of H₂CO and the T₁ and T₂ surfaces of acetylene. *J.
521 Comput. Chem.* **2002**, 23, 576-583.
- 522 15. Baker, J.; Wolinski, K., Isomerization of stilbene using enforced geometry optimization. *J. Comput.
523 Chem.* **2011**, 32, 43-53.
- 524 16. Zimmerman, P. M., Automated discovery of chemically reasonable elementary reaction steps. *J.
525 Comput. Chem.* **2013**, 34, 1385-1392.
- 526 17. Zimmerman, P. M., Growing string method with interpolation and optimization in internal
527 coordinates: Method and examples. *J. Chem. Phys.* **2013**, 138, 184102.
- 528 18. Zimmerman, P., Reliable Transition State Searches Integrated with the Growing String Method. *J.
529 Chem. Theory Comput.* **2013**, 9, 3043-3050.

- 530 19. Zimmerman, P. M., Single-ended transition state finding with the growing string method. *J. Comput.*
531 *Chem.* **2015**, *36*, 601-611.
- 532 20. Zimmerman, P. M., Navigating molecular space for reaction mechanisms: an efficient, automated
533 procedure. *Mol. Simul.* **2015**, *41*, 43-54.
- 534 21. Jafari, M.; Zimmerman, P. M., Reliable and efficient reaction path and transition state finding for
535 surface reactions with the growing string method. *J. Comput. Chem.* **2017**, *38*, 645-658.
- 536 22. Dewyer, A. L.; Zimmerman, P. M., Finding reaction mechanisms, intuitive or otherwise. *Org. &*
537 *Biomol. Chem.* **2017**, *15*, 501-504.
- 538 23. Rappoport, D.; Galvin, C. J.; Zubarev, D. Y.; Aspuru-Guzik, A., Complex Chemical Reaction Networks
539 from Heuristics-Aided Quantum Chemistry. *J. Chem. Theory Comput.* **2014**, *10*, 897-907.
- 540 24. Schaefer, B.; Mohr, S.; Amsler, M.; Goedecker, S., Minima hopping guided path search: An efficient
541 method for finding complex chemical reaction pathways. *J. Chem. Phys.* **2014**, *140*, 214102.
- 542 25. Wales, D. J., Perspective: Insight into reaction coordinates and dynamics from the potential energy
543 landscape. *J. Chem. Phys.* **2015**, *142*, 130901.
- 544 26. Habershon, S., Sampling reactive pathways with random walks in chemical space: Applications to
545 molecular dissociation and catalysis. *J. Chem. Phys.* **2015**, *143*, 094106.
- 546 27. Habershon, S., Automated Prediction of Catalytic Mechanism and Rate Law Using Graph-Based
547 Reaction Path Sampling. *J. Chem. Theory Comput.* **2016**, *12*, 1786-1798.
- 548 28. Zhang, X.-J.; Liu, Z.-P., Reaction sampling and reactivity prediction using the stochastic surface
549 walking method. *Phys. Chem. Chem. Phys.* **2015**, *17*, 2757-2769.
- 550 29. Wang, L.-P.; McGibbon, R. T.; Pande, V. S.; Martinez, T. J., Automated Discovery and Refinement of
551 Reactive Molecular Dynamics Pathways. *J. Chem. Theory Comput.* **2016**, *12*, 638-649.
- 552 30. Wang, L.-P.; Titov, A.; McGibbon, R.; Liu, F.; Pande, V. S.; Martínez, T. J., Discovering chemistry with
553 an ab initio nanoreactor. *Nat. Chem.* **2014**, *6*, 1044.
- 554 31. Yang, M.; Zou, J.; Wang, G.; Li, S., Automatic Reaction Pathway Search via Combined Molecular
555 Dynamics and Coordinate Driving Method. *J. Phys. Chem. A* **2017**, *121*, 1351-1361.
- 556 32. Jacobson, L. D.; Bochevarov, A. D.; Watson, M. A.; Hughes, T. F.; Rinaldo, D.; Ehrlich, S.; Steinbrecher,
557 T. B.; Vaitheeswaran, S.; Philipp, D. M.; Halls, M. D.; Friesner, R. A., Automated Transition State Search
558 and Its Application to Diverse Types of Organic Reactions. *J. Chem. Theory Comput.* **2017**, *13*, 5780-
559 5797.
- 560 33. Ohno, K.; Maeda, S., A Scaled Hypersphere Search Method for the Topography of Reaction Pathways
561 on the Potential Energy Surface. *Chem. Phys. Lett.* **2004**, *384*, 277-282.
- 562 34. Maeda, S.; Ohno, K., Global Mapping of Equilibrium and Transition Structures on Potential Energy
563 Surfaces by the Scaled Hypersphere Search Method: Applications to ab Initio Surfaces of
564 Formaldehyde and Propyne Molecules. *J. Phys. Chem. A* **2005**, *109*, 5742-5753.
- 565 35. Ohno, K.; Maeda, S., Global Reaction Route Mapping on Potential Energy Surfaces of Formaldehyde,
566 Formic Acid, and Their Metal-Substituted Analogues. *J. Phys. Chem. A* **2006**, *110*, 8933-8941.
- 567 36. Ohno, K.; Maeda, S., Automated Exploration of Reaction Channels. *Phys. Scr.* **2008**, *78*, 058122.
- 568 37. Maeda, S.; Morokuma, K., Communications: A systematic method for locating transition structures of
569 $A+B \rightarrow X$ type reactions. *J. Chem. Phys.* **2010**, *132*, 241102.
- 570 38. Maeda, S.; Morokuma, K., Finding Reaction Pathways of Type $A + B \rightarrow X$: Toward Systematic
571 Prediction of Reaction Mechanisms. *J. Chem. Theory Comput.* **2011**, *7*, 2335-2345.
- 572 39. Maeda, S.; Ohno, K.; Morokuma, K., Systematic exploration of the mechanism of chemical reactions:
573 the global reaction route mapping (GRRM) strategy using the ADDF and AFIR methods. *Phys. Chem.*
574 *Chem. Phys.* **2013**, *15*, 3683-3701.
- 575 40. Maeda, S.; Taketsugu, T.; Morokuma, K., Exploring transition state structures for intramolecular
576 pathways by the artificial force induced reaction method. *J. Comput. Chem.* **2014**, *35*, 166-173.
- 577 41. Maeda, S.; Harabuchi, Y.; Takagi, M.; Taketsugu, T.; Morokuma, K., Artificial Force Induced Reaction
578 (AFIR) Method for Exploring Quantum Chemical Potential Energy Surfaces. *Chem. Rec.* **2016**, *16*, 2232-
579 2248.
- 580 42. Maeda, S.; Harabuchi, Y.; Takagi, M.; Saita, K.; Suzuki, K.; Ichino, T.; Sumiya, Y.; Sugiyama, K.; Ono,
581 Y., Implementation and performance of the artificial force induced reaction method in the GRRM17
582 program. *J. Comput. Chem.* **2017**, DOI: 10.1002/jcc.25106.

- 583 43. Varela, J. A.; Vazquez, S. A.; Martínez-Núñez, E., An automated method to find reaction mechanisms
584 and solve the kinetics in organometallic catalysis. *Chem. Sci.* **2017**, *8*, 3843-3851.
- 585 44. Martínez-Núñez, E., An automated transition state search using classical trajectories initialized at
586 multiple minima. *Phys. Chem. Chem. Phys.* **2015**, *17*, 14912-14921.
- 587 45. Martínez-Núñez, E., An automated method to find transition states using chemical dynamics
588 simulations. *J. Comput. Chem.* **2015**, *36*, 222-234.
- 589 46. Rodríguez, A.; Rodríguez-Fernández, R.; A. Vázquez, S.; L. Barnes, G.; J. P. Stewart, J.; Martínez-
590 Núñez, E., tsscds2018: A code for automated discovery of chemical reaction mechanisms and solving
591 the kinetics. *Journal of Computational Chemistry* **2018**, *39*, 1922-1930.
- 592 47. Rodríguez, A.; Rodríguez-Fernández, R.; Vazquez, S. A.; Barnes, G. L.; Stewart, J. J. P.; Martínez-
593 Núñez, E. *tsscds2018*, <http://forge.cesga.es/wiki/g/tsscds/HomePage>.
- 594 48. Broadbelt, L. J.; Stark, S. M.; Klein, M. T., Computer Generated Pyrolysis Modeling: On-the-Fly
595 Generation of Species, Reactions, and Rates. *Ind. Eng. Chem. Res.* **1994**, *33*, 790-799.
- 596 49. Matheu, D. M.; Dean, A. M.; Grenda, J. M.; Green, W. H., Mechanism Generation with Integrated
597 Pressure Dependence: A New Model for Methane Pyrolysis. *J. Phys. Chem. A* **2003**, *107*, 8552-8565.
- 598 50. Gao, C. W.; Allen, J. W.; Green, W. H.; West, R. H., Reaction Mechanism Generator: Automatic
599 construction of chemical kinetic mechanisms. *Comput. Phys. Commun.* **2016**, *203*, 212-225.
- 600 51. Bhoorasingh, P. L.; West, R. H., Transition state geometry prediction using molecular group
601 contributions. *Phys. Chem. Chem. Phys.* **2015**, *17*, 32173-32182.
- 602 52. Bhoorasingh, P. L.; Slakman, B. L.; Seyedzadeh Khanshan, F.; Cain, J. Y.; West, R. H., Automated
603 Transition State Theory Calculations for High-Throughput Kinetics. *J. Phys. Chem. A* **2017**, *121*, 6896-
604 6904.
- 605 53. Suleimanov, Y. V.; Green, W. H., Automated Discovery of Elementary Chemical Reaction Steps Using
606 Freezing String and Berny Optimization Methods. *J. Chem. Theory Comput.* **2015**, *11*, 4248-4259.
- 607 54. Bergeler, M.; Simm, G. N.; Proppe, J.; Reiher, M., Heuristics-Guided Exploration of Reaction
608 Mechanisms. *J. Chem. Theory Comput.* **2015**, *11*, 5712-5722.
- 609 55. Proppe, J.; Husch, T.; Simm, G. N.; Reiher, M., Uncertainty quantification for quantum chemical
610 models of complex reaction networks. *Faraday Discuss.* **2016**, *195*, 497-520.
- 611 56. Simm, G. N.; Reiher, M., Context-Driven Exploration of Complex Chemical Reaction Networks. *J.*
612 *Chem. Theor. Comput.* **2017**, *13*, 6108-6119.
- 613 57. Simm, G. N.; Reiher, M., Error-Controlled Exploration of Chemical Reaction Networks with Gaussian
614 Processes. *J. Chem. Theor. Comput.* **2018**, *14*, 5238-5248.
- 615 58. Dewyer, A. L.; Argüelles, A. J.; Zimmerman, P. M., Methods for exploring reaction space in molecular
616 systems. *WIREs Comput Mol Sci* **2018**, *8*:e1354, doi: 10.1002/wcms.1354.
- 617 59. Eyring, H., The Activated Complex in Chemical Reactions. *J. Chem. Phys.* **1935**, *3*, 107-115.
- 618 60. Wigner, E., The transition state method. *Trans. Faraday Soc.* **1938**, *34*, 29-41.
- 619 61. Keck, J. C., Variational Theory of Reaction Rates. *Adv. Chem. Phys.* **1967**, *13*, 85-121.
- 620 62. Pechukas, P., Dynamics of Molecular Collisions. Plenum: New York, 1976.
- 621 63. Baker, J., An algorithm for the location of transition states. *J. Comput. Chem.* **1986**, *7*, 385-395.
- 622 64. Fukui, K., The Path of Chemical Reactions-The IRC Approach. *Acc. Chem. Res.* **1981**, *14*, 363.
- 623 65. Gillespie, D. T., A general method for numerically simulating the stochastic time evolution of coupled
624 chemical reactions. *J. Comput. Phys.* **1976**, *22*, 403-434.
- 625 66. Ferro-Costas, D.; Martínez-Núñez, E.; Rodríguez-Otero, J.; Cabaleiro-Lago, E.; Estévez, C. M.;
626 Fernández, B.; Fernández-Ramos, A.; Vázquez, S. A., Influence of Multiple Conformations and Paths
627 on Rate Constants and Product Branching Ratios. Thermal Decomposition of 1-Propanol Radicals. *J.*
628 *Phys. Chem. A* **2018**, *122*, 4790-4800.
- 629 67. Fenard, Y.; Gil, A.; Vanhove, G.; Carstensen, H.-H.; Van Geem, K. M.; Westmoreland, P. R.; Herbinet,
630 O.; Battin-Leclerc, F., A model of tetrahydrofuran low-temperature oxidation based on theoretically
631 calculated rate constants. *Combustion and Flame* **2018**, *191*, 252-269.
- 632 68. Wilhelm, M. J.; Martínez-Núñez, E.; González-Vázquez, J.; Vázquez, S. A.; Smith, J. M.; Dai, H.-L., Is
633 Photolytic Production a Viable Source of HCN and HNC in Astrophysical Environments? A
634 Laboratory-based Feasibility Study of Methyl Cyanofornate. *The Astrophysical Journal* **2017**, *849*, 15.

- 635 69. Perez-Soto, R.; Vazquez, S. A.; Martinez-Nunez, E., Photodissociation of acryloyl chloride at 193 nm:
636 interpretation of the product energy distributions, and new elimination pathways. *Phys. Chem. Chem.*
637 *Phys.* **2016**, *18*, 5019-5026.
- 638 70. Vazquez, S. A.; Martinez-Nunez, E., HCN elimination from vinyl cyanide: product energy
639 partitioning, the role of hydrogen-deuterium exchange reactions and a new pathway. *Phys. Chem.*
640 *Chem. Phys.* **2015**, *17*, 6948-6955.
- 641 71. Rossich Molina, E.; Salpin, J.-Y.; Spezia, R.; Martinez-Nunez, E., On the gas phase fragmentation of
642 protonated uracil: a statistical perspective. *Phys. Chem. Chem. Phys.* **2016**, *18*, 14980-14990.
- 643 72. Simm, G. N.; Vaucher, A. C.; Reiher, M., Exploration of Reaction Pathways and Chemical
644 Transformation Networks. *J. Phys. Chem. A* **2018**, doi: 10.1021/acs.jpca.8b10007.
- 645 73. Hase, W. L.; Buckowski, D. G., Monte carlo sampling of a microcanonical ensemble of classical
646 harmonic oscillators. *Chemical Physics Letters* **1980**, *74*, 284-287.
- 647 74. Bougueroua, S.; Spezia, R.; Pezzotti, S.; Vial, S.; Quessette, F.; Barth, D.; Gageot, M.-P., Graph theory
648 for automatic structural recognition in molecular dynamics simulations. *J. Chem. Phys.* **2018**, *149*,
649 184102.
- 650 75. Stewart, J. J. P. MOPAC2016, Stewart Computational Chemistry: Colorado Springs, CO, USA,
651 [HTTP://OpenMOPAC.net](http://OpenMOPAC.net), 2016.
- 652 76. Frisch, M. J.; Trucks, G. W.; Schlegel, H. B.; Scuseria, G. E.; Robb, M. A.; Cheeseman, J. R.; Scalmani,
653 G.; Barone, V.; Mennucci, B.; Petersson, G. A.; et al; Gaussian 09 revision A.02; Gaussian Inc.:
654 Wallingford CT, 2009.
- 655 77. Pietrucci, F.; Andreoni, W., Graph Theory Meets Ab Initio Molecule Dynamics: Atomic Structures and
656 Transformations at the Nanoscale. *Phys. Rev. Lett.* **2011**, *107*, 085504.
- 657 78. Smith, G.; Gilbert, R. G., Theory of unimolecular and recombination reactions. Blackwell Scientific
658 Publications: Oxford, 1990.
- 659 79. Tarrazo-Antelo, T.; Martinez-Nunez, E.; Vazquez, S. A., Ab initio and RRKM study of the elimination
660 of HF and HCl from chlorofluoroethylene. *Chem. Phys. Lett.* **2007**, *435*, 176-181.
- 661 80. Martínez-Núñez, E.; Vázquez, S., Rotational distributions of HBr in the photodissociation of vinyl
662 bromide at 193 nm: An investigation by direct quasiclassical trajectory calculations. *Chem. Phys. Lett.*
663 **2006**, *425*, 22.
- 664 81. Martínez-Núñez, E.; Vázquez, S., Quasiclassical trajectory calculations on the photodissociation of C
665 F₂CHCl at 193 nm: Product energy distributions for the HF and HCl eliminations. *J. Chem. Phys.* **2005**,
666 *122*, 1.
- 667 82. Martínez-Núñez, E.; Vázquez, S. A.; Aoiz, F. J.; Bañares, L.; Castillo, J. F., Further investigation of the
668 HCl elimination in the photodissociation of vinyl chloride at 193 nm: A direct MP2/6-31G(d,p)
669 trajectory study. *Chem. Phys. Lett.* **2004**, *386*, 225.
- 670 83. Martínez-Núñez, E.; Vázquez, S., Rovibrational distributions of HF in the photodissociation of vinyl
671 fluoride at 193 nm: A direct MP2 quasiclassical trajectory study. *J. Chem. Phys.* **2004**, *121*, 5179.
- 672 84. Martínez-Núñez, E.; Fernández-Ramos, A.; Vázquez, S. A.; JavierAoiz, F.; Bañares, L., A Direct
673 Classical Trajectory Study of HCl Elimination from the 193 nm Photodissociation of Vinyl Chloride. *J.*
674 *Phys. Chem. A* **2003**, *107*, 7611.
- 675 85. Gonzalez-Vazquez, J.; Martinez-Nunez, E.; Fernandez-Ramos, A.; Vazquez, S. A., Dissociation of
676 difluoroethylenes. II. Direct Classical Trajectory Study of the HF elimination from 1,2-
677 difluoroethylene. *J. Phys. Chem. A* **2003**, *107*, 1398-1404.
- 678 86. Gonzalez-Vazquez, J.; Fernandez-Ramos, A.; Martinez-Nunez, E.; Vazquez, S. A., Dissociation of
679 difluoroethylenes. I. Global potential energy surface, RRKM, and VTST calculations. *J. Phys. Chem. A*
680 **2003**, *107*, 1389-1397.
- 681 87. Martínez-Núñez, E.; Estévez, C. M.; Flores, J. R.; Vázquez, S. A., Product energy distributions for the
682 four-center HF elimination from 1,1-difluoroethylene. a direct dynamics study. *Chem. Phys. Lett.* **2001**,
683 *348*, 81.
- 684 88. Martínez-Núñez, E.; Vázquez, S. A., Three-center vs. four-center HF elimination from vinyl fluoride:
685 A direct dynamics study. *Chem. Phys. Lett.* **2000**, *332*, 583.
- 686 89. Homayoon, Z.; Vázquez, S. A.; Rodríguez-Fernández, R.; Martínez-Núñez, E., Ab initio and RRKM
687 study of the HCN/HNC elimination channels from vinyl cyanide. *J. Phys. Chem. A* **2011**, *115*, 979-985.

- 688 90. Martinez-Nunez, E.; Vazquez, S. A.; Borges, I.; Rocha, A. B.; Estevez, C. M.; Castillo, J. F.; Aoiz, F. J.,
689 On the conformational memory in the photodissociation of formic acid. *The Journal of Physical*
690 *Chemistry A* **2005**, 109, 2836-2839.
- 691 91. Martinez-Nunez, E.; Vazquez, S.; Granucci, G.; Persico, M.; Estevez, C. M., Photodissociation of formic
692 acid: A trajectory surface hopping study. *Chemical Physics Letters* **2005**, 412, 35-40.
- 693 92. Chang, C. M.; Huang, Y. H.; Liu, S. Y.; Lee, Y. P.; Pombar-Perez, M.; Martinez-Nunez, E.; Vazquez, S.
694 A., Internal energy of HCl upon photolysis of 2-chloropropene at 193 nm investigated with time-
695 resolved Fourier-transform spectroscopy and quasiclassical trajectories. *Journal of Chemical Physics*
696 **2008**, 129.
- 697 93. Spezia, R.; Martínez-Nuñez, E.; Vazquez, S.; Hase, W. L., Theoretical and computational studies of
698 non-equilibrium and non-statistical dynamics in the gas phase, in the condensed phase and at
699 interfaces. *Philosophical Transactions of the Royal Society A: Mathematical,*
700 *Physical and Engineering Sciences* **2017**, 375, 20170035.
- 701 94. Tsutsumi, T.; Harabuchi, Y.; Ono, Y.; Maeda, S.; Taketsugu, T., Analyses of trajectory on-the-fly based
702 on the global reaction route map. *Phys. Chem. Chem. Phys.* **2018**, 20, 1364-1372.
- 703 95. Wilhelm, M. J.; Nikow, M.; Letendre, L.; Dai, H.-L., *J. Chem. Phys.* **2009**, 130, 044307.
- 704 96. Chin, C.-H.; Lee, S.-H., *J. Chem. Phys.* **2011**, 134, 044309.
- 705 97. Chaudhuri, C.; Lee, S.-H., *Phys. Chem. Chem. Phys.* **2011**, 13, 7312.
- 706 98. Lee, P.-W.; Scrape, P. G.; Butler, L. J.; Lee, Y.-P., Two HCl-Elimination Channels and Two CO-
707 Formation Channels Detected with Time-Resolved Infrared Emission upon Photolysis of Acryloyl
708 Chloride [CH₂CHC(O)Cl] at 193 nm. *J. Phys. Chem. A* **2015**, 119, 7293-7304.
- 709 99. Bauer, C. A.; Grimme, S., How to Compute Electron Ionization Mass Spectra from First Principles. *J.*
710 *Phys. Chem. A* **2016**, 120, 3755-3766.
- 711 100. Macaluso, V.; Homayoon, Z.; Spezia, R.; Hase, W. L., Threshold for shattering fragmentation in
712 collision-induced dissociation of the doubly protonated tripeptide TIK(H⁺)₂. *Phys. Chem. Chem. Phys.*
713 **2018**, 20, 19744-19749.
- 714 101. Martin-Somer, A.; Martens, J.; Grzetic, J.; Hase, W. L.; Oomens, J.; Spezia, R., Unimolecular
715 Fragmentation of Deprotonated Diproline [Pro₂-H]⁻ Studied by Chemical Dynamics Simulations and
716 IRMPD Spectroscopy. *J. Phys. Chem. A* **2018**, 122, 2612-2625.
- 717 102. Homayoon, Z.; Macaluso, V.; Martin-Somer, A.; Muniz, M. C. N. B.; Borges, I.; Hase, W. L.; Spezia, R.,
718 Chemical dynamics simulations of CID of peptide ions: comparisons between TIK(H⁺)₂ and TLK(H⁺)₂
719 fragmentation dynamics, and with thermal simulations. *Phys. Chem. Chem. Phys.* **2018**, 20, 3614-3629.
- 720 103. Martin-Somer, A.; Spezia, R.; Yáñez, M., Gas-phase reactivity of [Ca(formamide)]₂⁺ complex: an
721 example of different dynamical behaviours. *Phil. Trans. R. Soc. A* **2017**, 375, 20160196.
- 722 104. Molina, E. R.; Eizaguirre, A.; Haldys, V.; Urban, D.; Doisneau, G.; Bourdreux, Y.; Beau, J.-M.; Salpin,
723 J.-Y.; Spezia, R., Characterization of Protonated Model Disaccharides from Tandem Mass Spectrometry
724 and Chemical Dynamics Simulations. *ChemPhysChem* **2017**, 18, 2812-2823.
- 725 105. Lee, G.; Park, E.; Chung, H.; Jeanvoine, Y.; Song, K.; Spezia, R., Gas phase fragmentation mechanisms
726 of protonated testosterone as revealed by chemical dynamics simulations. *Int. J. Mass Spectrom.* **2016**,
727 407, 40-50.
- 728 106. Spezia, R.; Lee, S. B.; Cho, A.; Song, K., Collision-induced dissociation mechanisms of protonated
729 penta- and octa-glycine as revealed by chemical dynamics simulations. *Int. J. Mass Spectrom.* **2015**,
730 392, 125-138.
- 731 107. Spezia, R.; Martens, J.; Oomens, J.; Song, K., Collision-induced dissociation pathways of protonated
732 Gly₂NH₂ and Gly₃NH₂ in the short time-scale limit by chemical dynamics and ion spectroscopy. *Int.*
733 *J. Mass Spectrom.* **2015**, 388, 40-52.
- 734 108. Song, K.; Spezia, R., *Theoretical Mass Spectrometry, Tracing Ions with Classical Trajectories.* De
735 Gruyter: Berlin, Boston, 2018.
- 736 109. Pratihari, S.; Barnes, G. L.; Laskin, J.; Hase, W. L., Dynamics of Protonated Peptide Ion Collisions with
737 Organic Surfaces: Consonance of Simulation and Experiment. *J. Phys. Chem. Lett.* **2016**, 7, 3142-3150.
- 738 110. Pratihari, S.; Barnes, G. L.; Hase, W. L., Chemical dynamics simulations of energy transfer, surface-
739 induced dissociation, soft-landing, and reactive-landing in collisions of protonated peptide ions with
740 organic surfaces. *Chem. Soc. Rev.* **2016**, 45, 3595-3608.

- 741 111. Barnes, G. L.; Young, K.; Yang, L.; Hase, W. L., Fragmentation and reactivity in collisions of protonated
742 diglycine with chemically modified perfluorinated alkylthiolate-self-assembled monolayer surfaces. *J.*
743 *Chem. Phys.* **2011**, *134*, 094106.
- 744 112. Park, K.; Deb, B.; Song, K.; Hase, W. L., Importance of Shattering Fragmentation in the Surface-Induced
745 Dissociation of Protonated Octaglycine. *JASMS* **2009**, *20*, 939-948.
- 746 113. Barnes, G. L.; Hase, W. L., Energy Transfer, Unfolding, and Fragmentation Dynamics in Collisions of
747 N-Protonated Octaglycine with an H-SAM Surface. *J. Am. Chem. Soc.* **2009**, *131*, 17185-17193.
- 748 114. Martínez-Núñez, E.; Fernández-Ramos, A.; Vázquez, S. A.; Marques, J. M. C.; Xue, M.; Hase, W. L.,
749 Quasiclassical dynamics simulation of the collision-induced dissociation of Cr (CO)₆ + with Xe. *J.*
750 *Chem. Phys.* **2005**, *123*, 154311.
- 751 115. Zador, J.; Jasper, A. W.; Miller, J. A., The reaction between propene and hydroxyl. *Phys. Chem. Chem.*
752 *Phys.* **2009**, *11*, 11040-11053.
- 753 116. Zhou, C.-W.; Li, Z.-R.; Li, X.-Y., Kinetics and Mechanism for Formation of Enols in Reaction of
754 Hydroxide Radical with Propene. *J. Phys. Chem. A* **2009**, *113*, 2372-2382.
- 755 117. Huynh, L. K.; Zhang, H. R.; Zhang, S.; Eddings, E.; Sarofim, A.; Law, M. E.; Westmoreland, P. R.;
756 Truong, T. N., Kinetics of Enol Formation from Reaction of OH with Propene. *J. Phys. Chem. A* **2009**,
757 *113*, 3177-3185.
- 758 118. El-Nahas, A. M.; Uchamaru, T.; Sugie, M.; Tokuhashi, K.; Sekiya, A., Relative reactivity and
759 regioselectivity of halogen-substituted ethenes and propene toward addition of an OH radical or O
760 (3P) atom: An ab initio study. *THEOCHEM* **2006**, *770*, 59-65.
- 761 119. Szori, M.; Fittschen, C.; Csizmadia, I. G.; Viskolcz, B., Allylic H-Abstraction Mechanism: The Potential
762 Energy Surface of the Reaction of Propene with OH Radical. *J. Chem. Theor. Comput.* **2006**, *2*, 1575-
763 1586.
- 764 120. Díaz-Acosta, I.; Alvarez-Idaboy, J. R.; Vivier-Bunge, A., Mechanism of the OH-propene-O₂ reaction:
765 An ab initio study. *Int. J. Chem. Kinet.* **1999**, *31*, 29-36.
- 766 121. Alvarez-Idaboy, J. R.; Díaz-Acosta, I.; Vivier-Bunge, A., Energetics of mechanism of OH-propene
767 reaction at low pressures in inert atmosphere. *J. Comput. Chem.* **1998**, *19*, 811-819.
- 768 122. Ferro-Costas, D.; Cordeiro, M. N. D. S.; Truhlar, D. G.; Fernández-Ramos, A., Q2DTor: A program to
769 treat torsional anharmonicity through coupled pair torsions in flexible molecules. *Computer Physics*
770 *Communications* **2018**, *232*, 190-205.
- 771 123. Truhlar, D. G.; Isaacson, A. D.; Garret, G. C., *Theory of Chemical Reaction Dynamics*. Baer, M., Ed.
772 CRC: Boca Raton, FL, 1985; Vol. 4, p 65.
- 773 124. Schwarz, H., *Chemistry with Methane: Concepts Rather than Recipes*. *Angew. Chem. Int. Ed.* **2011**, *50*,
774 10096-10115.
- 775 125. Bao, J. L.; Truhlar, D. G., Variational transition state theory: theoretical framework and recent
776 developments. *Chem. Soc. Rev.* **2017**, *46*, 7548-7596.
- 777 126. Yu, T.; Zheng, J.; Truhlar, D. G., Multi-structural variational transition state theory. Kinetics of the 1,4-
778 hydrogen shift isomerization of the pentyl radical with torsional anharmonicity. *Chem. Sci.* **2011**, *2*,
779 2199-2213.
- 780 127. Bao, J. L.; Meana-Pañeda, R.; Truhlar, D. G., Multi-path variational transition state theory for chiral
781 molecules: the site-dependent kinetics for abstraction of hydrogen from 2-butanol by hydroperoxyl
782 radical, analysis of hydrogen bonding in the transition state, and dramatic temperature dependence of
783 the activation energy. *Chemical Science* **2015**, *6*, 5866-5881.
- 784 128. Yu, T.; Zheng, J.; Truhlar, D. G., Multipath Variational Transition State Theory: Rate Constant of the
785 1,4-Hydrogen Shift Isomerization of the 2-Cyclohexylethyl Radical. *J. Phys. Chem. A* **2012**, *116*, 297-
786 308.
- 787 129. Meana-Pañeda, R.; Fernández-Ramos, A., Accounting for conformational flexibility and torsional
788 anharmonicity in the H + CH₃CH₂OH hydrogen abstraction reactions: A multi-path variational
789 transition state theory study. *The Journal of Chemical Physics* **2014**, *140*, 174303.
- 790 130. Sperger, T.; Sanhueza, I. A.; Schoenebeck, F., Computation and Experiment: A Powerful Combination
791 to Understand and Predict Reactivities. *Acc. Chem. Res.* **2016**, *49*, 1311-1319.
- 792 131. Peng, Q.; Paton, R. S., Catalytic Control in Cyclizations: From Computational Mechanistic
793 Understanding to Selectivity Prediction. *Acc. Chem. Res.* **2016**, *49*, 1042-1051.

- 794 132. Sperger, T.; Sanhueza, I. A.; Kalvet, I.; Schoenebeck, F., Computational Studies of Synthetically
795 Relevant Homogeneous Organometallic Catalysis Involving Ni, Pd, Ir, and Rh: An Overview of
796 Commonly Employed DFT Methods and Mechanistic Insights. *Chem. Rev.* **2015**, *115*, 9532-9586.
- 797 133. Rush, L. E.; Pringle, P. G.; Harvey, J. N., Computational Kinetics of Cobalt-Catalyzed Alkene
798 Hydroformylation. *Angew. Chem. Int. Ed.* **2014**, *53*, 8672-8676.
- 799 134. Maeda, S.; Morokuma, K., Toward Predicting Full Catalytic Cycle Using Automatic Reaction Path
800 Search Method: A Case Study on HCo(CO)₃-Catalyzed Hydroformylation. *J. Chem. Theor. Comput.*
801 **2012**, *8*, 380-385.
- 802 135. Kim, Y.; Choi, S.; Kim, W. Y., Efficient Basin-Hopping Sampling of Reaction Intermediates through
803 Molecular Fragmentation and Graph Theory. *J. Chem. Theory Comput.*, Article ASAP.
- 804 136. Kim, Y.; Kim, J. W.; Kim, Z.; Kim, W. Y., Efficient prediction of reaction paths through molecular graph
805 and reaction network analysis. *Chem. Sci.* **2018**, *9*, 825-835.
- 806 137. Heck, R. F.; Breslow, D. S., The Reaction of Cobalt Hydrotetracarbonyl with Olefins. *J. Am. Chem. Soc.*
807 **1961**, *83*, 4023-4027.
- 808 138. Gholap, R. V.; Kut, O. M.; Bourne, J. R., Hydroformylation of propylene using an unmodified cobalt
809 carbonyl catalyst: a kinetic study. *Ind. Eng. Chem. Res.* **1992**, *31*, 1597-1601.
- 810 139. Booth, J.; Vazquez, S.; Martínez-Núñez, E.; Marks, A.; Rodgers, J.; Glowacki, D. R.; Shalashilin, D. V.,
811 Recent Applications of Boxed Molecular Dynamics: a Simple Multiscale Technique for Atomistic
812 Simulations. *Phil. Trans. R. Soc. A* **2014**, *372*, 20130384.
- 813 140. Martínez-Núñez, E.; Shalashilin, D. V., Acceleration of classical mechanics by phase space constraints.
814 *J. Chem. Theor. Comput.* **2006**, *2*, 912.
- 815 141. Shannon, R. J.; Amabilino, S.; O'Connor, M.; Shalishilin, D. V.; Glowacki, D. R., Adaptively
816 Accelerating Reactive Molecular Dynamics Using Boxed Molecular Dynamics in Energy Space. *J.*
817 *Chem. Theor. Comput.* **2018**, *14*, 4541-4552.
- 818 142. Larsen, A. H.; Mortensen, J. J.; Blomqvist, J.; Castelli, I. E.; Christensen, R.; Dułak, M.; Friis, J.; Groves,
819 M. N.; Hammer, B.; Hargus, C.; Hermes, E. D.; Jennings, P. C.; Jensen, P. B.; Kermode, J.; Kitchin, J. R.;
820 Kolsbjerg, E. L.; Kubal, J.; Kaasbjerg, K.; Lysgaard, S.; Maronsson, J. B.; Maxson, T.; Olsen, T.; Pastewka,
821 L.; Peterson, A.; Rostgaard, C.; Schiøtz, J.; Schütt, O.; Strange, M.; Thygesen, K. S.; Vegge, T.;
822 Vilhelmsen, L.; Walter, M.; Zeng, Z.; Jacobsen, K. W., The atomic simulation environment—a Python
823 library for working with atoms. *Journal of Physics: Condensed Matter* **2017**, *29*, 273002.
- 824 143. Valiev, M.; Bylaska, E. J.; Govind, N.; Kowalski, K.; Straatsma, T. P.; Van Dam, H. J. J.; Wang, D.;
825 Nieplocha, J.; Apra, E.; Windus, T. L.; de Jong, W. A., NWChem: A comprehensive and scalable open-
826 source solution for large scale molecular simulations. *Comput. Phys. Commun.* **2010**, *181*, 1477-1489.
- 827 144. Neese, F., The ORCA program system. *Wiley Interdiscip. Rev. Comput. Mol. Sci.* **2012**, *2*, 73-78.
- 828 145. Christensen, A. S.; Kubař, T.; Cui, Q.; Elstner, M., Semiempirical Quantum Mechanical Methods for
829 Noncovalent Interactions for Chemical and Biochemical Applications. *Chemical Reviews* **2016**, *116*,
830 5301-5337.
- 831 146. Rodríguez-Fernández, R.; Pereira, F. B.; Marques, J. M. C.; Martínez-Núñez, E.; Vázquez, S. A., GAFit:
832 A general-purpose, user-friendly program for fitting potential energy surfaces. *Computer Physics*
833 *Communications* **2017**, *217*, 89-98.
- 834 147. Nogueira, J. J.; Sánchez-Coronilla, A.; Marques, J. M. C.; Hase, W. L.; Martínez-Núñez, E.; Vázquez, S.
835 A., Intermolecular potentials for simulations of collisions of SiNCS⁺ and (CH₃)₂SiNCS⁺ ions with
836 fluorinated self-assembled monolayers. *Chemical Physics* **2012**, *399*, 193-204.
- 837 148. Pratihari, S.; Kohale, S. C.; Vázquez, S. A.; Hase, W. L., Intermolecular Potential for Binding of
838 Protonated Peptide Ions with Perfluorinated Hydrocarbon Surfaces. *The Journal of Physical Chemistry*
839 *B* **2014**, *118*, 5577-5588.
- 840 149. arXiv:1806.06147 [physics.chem-ph]. arXiv:1806.06147 [physics.chem-ph].
- 841 150. Thomas, H. B.; Hennemann, M.; Kibies, P.; Hoffgaard, F.; Güssregen, S.; Hessler, G.; Kast, S. M.; Clark,
842 T., The hpCADD NDDO Hamiltonian: Parametrization. *Journal of Chemical Information and*
843 *Modeling* **2017**, *57*, 1907-1922.
- 844 151. Brooks, B. R.; Brooks, C. L., 3rd; Mackerell, A. D., Jr.; Nilsson, L.; Petrella, R. J.; Roux, B.; Won, Y.;
845 Archontis, G.; Bartels, C.; Boresch, S.; Cafilisch, A.; Caves, L.; Cui, Q.; Dinner, A. R.; Feig, M.; Fischer,
846 S.; Gao, J.; Hodosscek, M.; Im, W.; Kuczera, K.; Lazaridis, T.; Ma, J.; Ovchinnikov, V.; Paci, E.; Pastor, R.
847 W.; Post, C. B.; Pu, J. Z.; Schaefer, M.; Tidor, B.; Venable, R. M.; Woodcock, H. L.; Wu, X.; Yang, W.;

- 848 York, D. M.; Karplus, M., CHARMM: the biomolecular simulation program. *J. Comput. Chem.* **2009**,
849 30, 1545-1614.
- 850 152. Hase, W. L.; Bolton, K.; Sainte Claire, P. d.; Duchovic, R. J.; Hu, X.; Komornicki, A.; Li, G.; Lim, K. F.;
851 Lu, D.-H.; Peslherbe, G. H. et al.; Venus05; a general chemical dynamics computer program; 2004.
852